An EBG-Driven 2-Port MIMO Antenna Featuring Enhanced Isolation and Circular Polarization for IEEE 802.11ad JC&S Terminals

Shahanawaz Kamal, Mehrab Ramzan, and Padmanava Sen

Radio Frequency Design Enablement Group, Barkhausen Institut, 01067 Dresden, Germany
Emails: {shahanawaz.kamal, mehrab.ramzan, padmanava.sen}@barkhauseninstitut.org

***Abstract*—This paper addresses the issue of high cost and fabrication complexity associated with isolating circularly polarized (CP) waves in a compact multiple-input−multiple-output (MIMO) antenna for joint communications and sensing (JC&S) in IEEE 802.11ad spectrum. A printed circuit board (PCB)-based dual-port antenna engaging $3.83\lambda \times 3.83\lambda \times 0.04\lambda$ area at the center frequency of 57.55 GHz is proposed. The antenna comprises of a microstrip patch attached to a grounded coplanar waveguide (CPW), with a signal track designed to enable CP radiations. A metallic grid-based electromagnetic bandgap (EBG) structure was engineered and positioned between the two antenna elements to attain a peak isolation of 50.83 dB. The distance between each pair of microstrip parts was subjected to the fabrication capabilities of conventional PCB manufacturers. The final arrangement yielded a gain of ≈10 dBi and efficiency of >85%. The simulation results have been validated through cost-effective fabrication and measurements. Compared to the latest designs, the proposed antenna is fairly competitive.**

***Index Terms*—Cost-effective, circular polarization (CP), compact, efficiency, electromagnetic bandgap (EBG), gain, isolation, multiple-input−multiple-output (MIMO).**

I. Introduction

The throughput required for joint communications and sensing (JC&S) via radio, for instance three-dimensional high definition video streams and others has been exceeding the available capacity in sub-10 GHz spectrum [1], [2]. The IEEE 802.11ad standard for JC&S in the 60 GHz band offers multi-Gigabit rates to meet this requirement [3]. The 60 GHz band, which ranges from 57−71 GHz, is an unlicensed band that is available across the globe. This spectrum has the advantage of small wavelengths of about 5 mm, enabling the deployment of miniature antennas that are essential for handheld devices. However, there is a great deal of free space attenuation in the 60 GHz range [4].

Antennas with circularly polarized (CP) radiation pattern exhibit good absorption impairments, transmission gains, and reflection performances [5], [6]. Furthermore, CP antennas exhibit remarkable efficiency in mitigating signal attenuation resulting from environmental factors, including snow, precipitation and others. Another option to achieve higher throughput is to take advantage of multiplexing techniques by equipping the user phone with a second antenna [7], [8]. Therefore, CP multiple-input−multiple-output (MIMO) antennas would be a good choice to meet the throughput requirements of digital systems [9], [10]. However, the isolation problem that results in MIMO antennas eventually lowers the throughput performance [11]–[13]. Hence, it's critical to look for ways to improve the isolation between antenna elements.

Manufacturing compact antennas for the millimeter wave bands has proven quite expensive and complex [14], [15]. The use of printed circuit board (PCB) represents a low cost and easy fabrication method [16]. A PCB-based aperture coupled antenna for operation at 60 GHz was manufactured in [17]. However, the framework was made of multiple PCB layers that resulted in occupying a large profile. Moreover, the antenna involved distinct vias, adding to the design complexity. Similarly, an air cavity-based multi-layer organic package antenna for the 60 GHz band was fabricated in [18]. However, the air cavity in the layout complicated fabrication and increased the risk of delamination during high-temperature soldering. Furthermore, strict design guidelines for the copper-to-edge clearance, element spacing, and trace dimensions are vital for standard PCB production.

The fundamental goal of this work remained to establish a cost-effective method for isolating CP waves in small antennas. Particularly, we propose a PCB-based dual-port microstrip patch antenna that occupies $3.83\lambda \times 3.83\lambda \times 0.04\lambda$ area in IEEE 802.11ad spectrum. The proposed antenna leverages a strategically designed signal track of CPW to enable CP waves. A peak isolation of 50.83 dB was achieved by meticulously placing an EBG structure between the two antenna elements. Furthermore, reasonable MIMO antenna performance with gain of ≈10 dBi, efficiency of >85%, envelope correlation coefficient (ECC) of <0.5, and diversity gain (DG) of ≈10 dB was ascertained. The Ansys high frequency structure simulator (HFSS) simulation results have been verified through inexpensive fabrication and measurement.

II. Design Framework

A. Antenna Layout

Fig. 1(a−c) shows the proposed antenna configuration, and Table I lists their parameter values. The antenna was made up of two ports that fed from opposite ends. RO4350B™

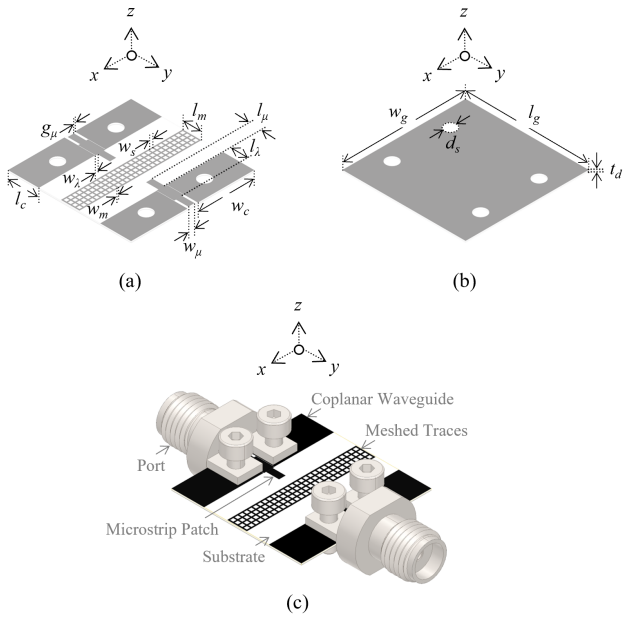

Fig. 1. Proposed antenna layouts: (a) Top, (b) bottom, and (c) perspective.

TABLE I
ANTENNA PARAMETER VALUES IN λ AT 57.55 GHZ.

Parameter	Value	Description
l_g	3.83	ground length
w_g	3.83	ground width
t_d	0.04	dielectric substrate thickness
d_s	0.19	screw diameter
l_c	1.76	coplanar waveguide length
w_c	0.96	coplanar waveguide width
l_μ	0.38	microstrip feed or patch length
w_μ	0.19	microstrip feed or patch width
l_λ	0.55	transition of feedline length
w_λ	0.06	transition of feedline width
l_m	0.58	meshed trace length
w_m	0.04	unit meshed trace width
w_s	0.09	unit meshed slot width
g_μ	0.07	gap among coplanar ground and feedline edge

PCB with dielectric constant (ϵ_r) of 3.48 $\pm$ 0.05, and loss tangent (tan δ) of 0.0037 was deployed. The bottom side of PCB was integrated with a full ground plane. Two CPW-fed microstrip patches positioned in front of one another and separated by meshed traces made up the top side of PCB. The spacing between every pair of microstrip portions was considered to be within the fabrication capabilities of standard PCB manufacturers.

B. Coplanar Waveguide

A CPW framework is typically comprised of one conducting (signal) track, and two return conductors (CPW-ground), one on each side of the track. The equations mentioned in [19] served as the basis for designing the standard CPW to match the port impedance. The calculated values were subsequently employed to model and simulate the traditional CPW in HFSS. A resonance from 57.3−57.7 GHz was accomplished, as displayed in Fig. 2(a). However, the axial ratio (AR) values were >3 dB, as illustrated in Fig. 2(a). The

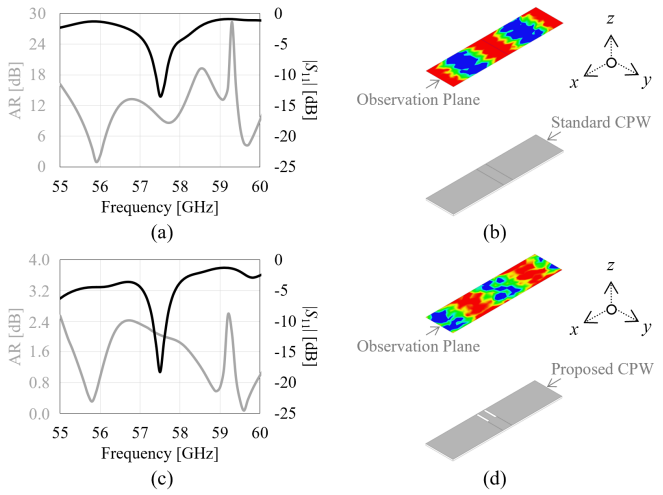

Fig. 2. Standard CPW results: (a) $|S_{11}|$ and AR, and (b) electric field at 57.55 GHz. Proposed CPW results: (c) $|S_{11}|$ and AR, and (d) electric field at 57.55 GHz.

electric field along an observation plane has been examined to ascertain the current distribution of the standard CPW at 57.55 GHz. The center of the arrangement showed the largest current distribution, indicated by the red color in Fig. 2(b). Hence, slots were inserted into the signal track to split the incident wave into two equal orthogonal components. An adequate impedance matching response, and AR of <3 dB was established with the proposed CPW design, as shown in Fig. 2(c). The enlarged gap between the CPW-ground and the feedline edge contributed in rerouting the currents, allowing two orthogonal resonant modes with identical amplitude and 90° phase deviation being induced, as depicted in Fig. 2(d).

C. Microstrip Patch

The bandwidth of the proposed CPW layout described in the previous subsection was only 0.4 GHz. Hence, a microstrip patch was introduced in juxtaposition with the signal track, the dimensions of which were determined using the calculations stated in [20]. The antenna operated from 56.7−58.4 GHz, allowing for an improvement of 1.3 GHz bandwidth through the integration of microstrip patch to the proposed CPW, as shown in Fig. 3(a). Furthermore, an AR of <3 dB was ascertained across the entire operating band, as demonstrated in Fig. 3(a). It is worth noting that an expanded impedance bandwidth may be produced by introducing new resonant frequencies with microstrip patches; however, this was not the objective of this study. Therefore, this CPW-fed single element microstrip patch antenna setup was considered as optimum.

To proceed on to the MIMO setup phase of the investigation, simulation studies were carried out where two CPW-fed microstrip patch antenna elements were positioned in front of each other. As displayed in Fig. 3(b), the CPW-fed dual element microstrip patch antenna provided >12 dB of isolation and <3 dB of AR in the working band from 56.7−58.4 GHz.

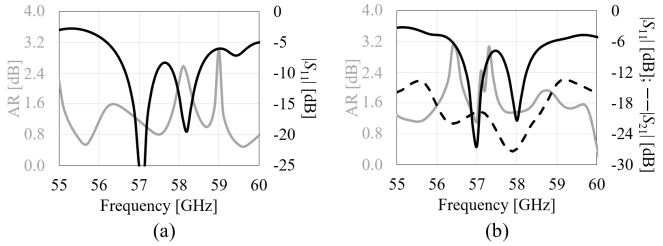

Fig. 3. (a) Proposed CPW-fed single element antenna results: $|S_{11}|$ and AR. (b) Proposed CPW-fed dual element antenna results: $|S_{11}|$, $|S_{21}|$ and AR.

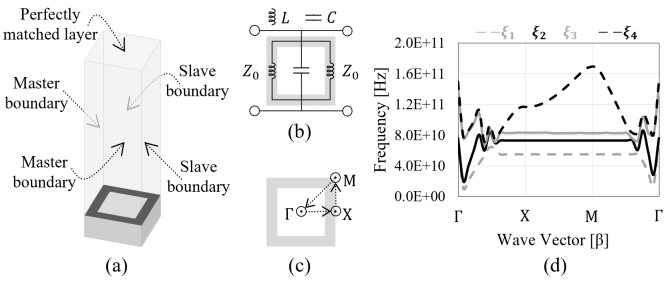

Fig. 4. Proposed unit EBG cell: (a) Layout, (b) equivalent circuit, (c) Brillouin region, and (d) dispersion diagram.

D. Meshed Traces

The CPW-fed dual element microstrip patch antenna configuration mentioned in the preceding subsection yielded a maximum isolation of only upto 24 dB. Consequently, meshed traces were modeled to achieve an EBG and placed between the two antenna elements to mitigate the mutual coupling effects. Based on the equations presented in [21], the dimensions of the unit EBG resonating in the 60 GHz spectrum were established. Subsequently, unit cell simulations were carried out utilizing the HFSS eigenmode solver. Fig. 4(a) depicts the unit cell diagram, which has periodic boundaries assigned to the unit cell to realize an array of the inductive metallic grid. During the simulation, four modes (ξ) were excited, and the structure's impedance response was recorded. The resonance characteristic was further verified using an equivalent circuit portrayed in Fig. 4(b), where the letters C and L represent, respectively, the inter-element spacing and the transmission line elements.

The Brillouin domain was taken into account while conducting the HFSS eigenmode simulation to assess the EBG property of the unit cell. The Γ position indicates the focal point of the Brillouin area, while the M and X positions constitute the intersections of an edge and a face, respectively, as shown in Fig. 4(c). The relationship between these points and the wave vector is expressed in [22]. The unit cell dimensions of the metallic grid were tuned such that it yields an EBG in the desired frequency band. This is confirmed by the results of the unit metallic grid in Fig. 4(d), which demonstrates a 17.5 GHz wide EBG from 55−72.5 GHz.

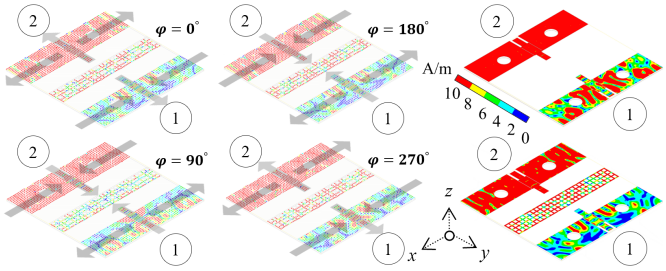

Fig. 5. Proposed antenna current distribution at 57.55 GHz.

III. Operating Principle

The working principle of proposed CPW-fed dual element microstrip patch antenna with meshed EBG traces has been analyzed by examining the current distribution at 57.55 GHz, as portrayed in the initial four photographs in Fig. 5. Understanding the current flow's trajectory—which is indicated with gray arrows for easily identifying the direction of the primary current flow—the proposed antenna established the CP mechanism. For instance, the principal currents on signal tracks near port 2 and port 1 were generated, respectively, in the directions of −y and +y at 0°, +y and −y at 90°, +y and −y at 180°, and −y and +y at 270°. Similarly, the fundamental currents on the CPW ground near port 2 were produced in the directions of −x and +x at 0°, +x and −x at 90°, +x and −x at 180°, and −x and +x at 270°. Furthermore, the primary currents on the CPW ground near port 1 were generated in the directions of +x and −x at 0°, −x and +x at 90°, −x and +x at 180°, and +x and −x at 270°.

The importance of meshed traces is confirmed by the surface current distribution at 57.55 GHz depicted in the rightmost two images in Fig. 5. Descriptively, the antenna without meshed traces showed a significant amount of coupling of the surface currents from port 2 into port 1, while the antenna with meshed traces confirmed a significant blockage of surface currents entering from port 2 to port 1.

IV. Experimental Validation

The simulation results were validated through measurements conducted in the anechoic chamber. Fig. 6(a−b) displays the fabricated antenna under measurement of S-parameters and radiation patterns. The simulation and measurement results showed a fair degree of agreement.

Fig. 7(a) displays the $|S_{11}|$ response of the proposed antenna. An appropriate −10 dB impedance matching from 56.7−58.4 GHz (1.7 GHz bandwidth) with 57.55 GHz center frequency was accomplished. The $|S_{21}|$ response of the proposed antenna is demonstrated Fig. 7(b). Peak isolation of 50.83 dB was established with the help of meshed EBG traces.

The AR response was examined to confirm the CP behavior that was found to be below the 3 dB range as depicted in Fig. 8(a). The gain response illustrated in Fig. 8(b) confirms that >7 dBi gain was attained in the entire operating frequency band. The simulated and measured right/left hand (R/LH) CP

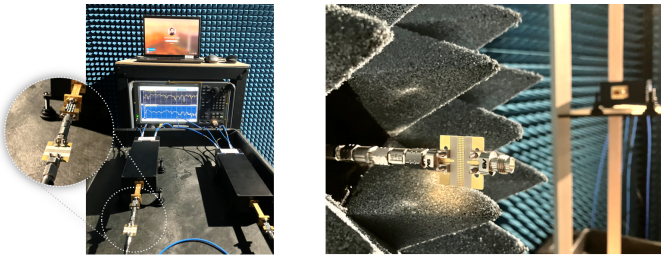

(a) (b)

Fig. 6. Proposed antenna experimental measurement setup of (a) *S*-parameters and (b) radiation patterns.

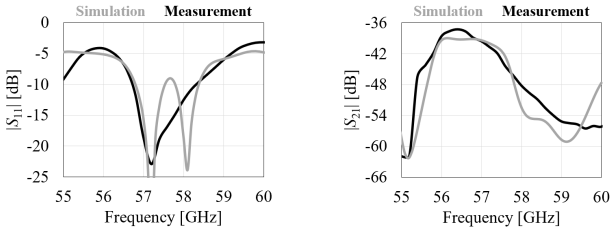

Fig. 7. Proposed antenna results: (a) $|S_{11}|$, and (b) $|S_{21}|$.

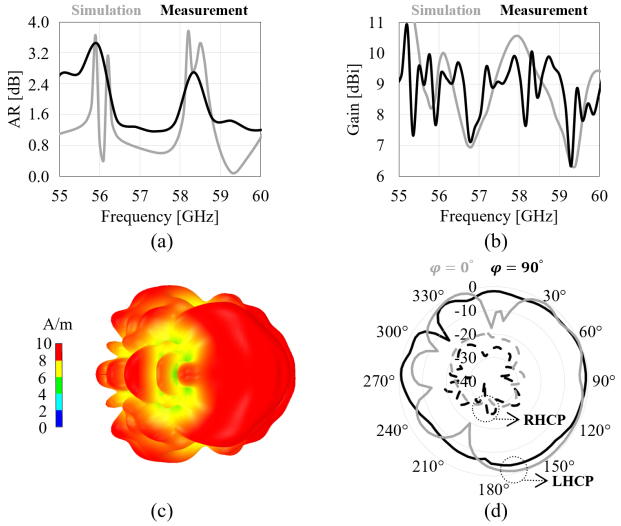

Fig. 8. Proposed antenna results: (a) AR, (b) gain, (c) simulated gain pattern at 57.55 GHz, and (d) measured radiation pattern at 57.55 GHz.

radiation patterns at 57.55 GHz is shown in Figs. 8(c) and 8(d), respectively. Stable radiation patterns were confirmed with a gain of 9.53 dBi at 57.55 GHz.

The antenna's good MIMO performance has been supported by ECC of $<$0.5 and DG of $\approx$10 dB, as illustrated in Fig. 9(a). The expressions mentioned in [23] were utilized to evaluate ECC and DG. Finally, reasonable efficiency of 86.82% at 57.55 GHz was confirmed, as displayed in Fig. 9(b).

V. Benchmarking

Table II presents a comparison between the proposed antenna and state-of-the-art antennas to highlight the importance

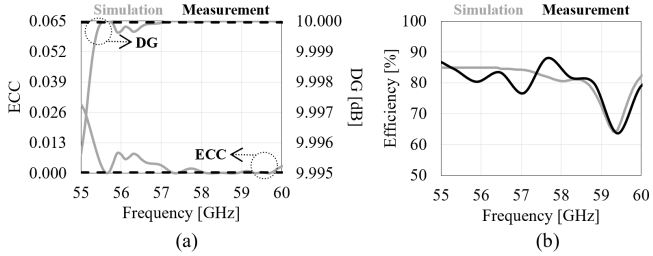

Fig. 9. Proposed antenna results: (a) ECC and DG, and (b) efficiency.

of this work. A down (↓) and an up (↑) arrow, respectively, have been used in the table to indicate a relatively poor performance measure and the necessity for a large area with high fabrication cost. In the context of an economically viable method to improve isolation between adjacent CP radiating elements, the proposed antenna configuration remains competitive. Similarly, the proposed antenna works reasonably within all of the remaining specifications factored into considerations. With respect to other antennas, the proposed antenna's impedance bandwidth tends to be small. However, accomplishing a broad bandwidth was not the goal of this research. Furthermore, an extended bandwidth may be achieved by adding new resonant frequencies via simple methods, as discussed in the design framework section.

VI. Conclusion

This paper presents the design of a cost-effective and compact MIMO antenna that generated high gain CP radiations at 57.55 GHz center frequency. In the CPW signal track, slots were added at key locations to achieve a compact geometry and CP radiations. Meshed traces were modeled to attain an EBG and integrated between the antenna elements to enhance isolation. The distance between each pair of microstrip sections was kept within the capabilities of standard PCB manufacturers. Therefore, the proposed antenna was fabricated at a cost-effective rate. This work delivers four significant advancements. First, the proposed layout of meshed traces produces a wide EBG. Second, the proposed MIMO antenna yields CP radiations with good efficiency and gain values. Thirdly, the proposed MIMO antenna and EBG structure have simple geometry. Finally, the proposed MIMO antenna and EBG configurations represent inexpensive methods to enhance port isolation. Hence, the proposed MIMO antenna represents a good fit for IEEE 802.11ad JC&S terminals.

Acknowledgment

The project on which this report is based was funded by the German Federal Ministry of Education and Research (BMBF) under the funding code 16MEE0248. The responsibility for the content of this publication lies with the author.

This work was also funded by the European Union (EU) under the funding code 101097296. Views and opinions expressed are however those of the author(s) only and do not necessarily reflect those of the EU. Neither the EU nor the granting authority can be held responsible for them.

TABLE II
PERFORMANCE SUMMARY OF STATE-OF-THE-ART ANTENNAS.

Antenna fabrication technology	Layout	Dimension (λ^2)	Profile (λ)	Frequency (GHz)	Bandwidth (%)	Polarization	Isolation (dB)	Gain (dBi)	Efficiency (%)	Reference
Metallic nanowire membrane ↑	Array	0.84 × 0.84	0.01	60.00	12.20	Linear ↓	9.20 ↓	−6.90 ↓	—	[24]
Multiple substrates and metals ↑	Array	5.77 × 5.77 ↑	0.46 ↑	58.00	16.10	Circular	—	20.00	52.40 ↓	[25]
Multiple substrates and spacers ↑	MIMO	5.36 × 3.07 ↑	0.32 ↑	59.00	23.70	Linear ↓	53.00	8.50 ↓	89.00	[26]
Multiple printed circuit boards ↑	MIMO	3.00 × 3.00	1.00 ↑	59.50	11.76	Circular	15.00 ↓	−5.00 ↓	55.00 ↓	[27]
Single printed circuit board	MIMO	3.83 × 3.83	0.04	57.55	2.95	Circular	50.83	9.53	86.82	This work

↑ represents a high fabrication cost or large size in comparison to the proposed antenna. ↓ conveys poor performance relative to the proposed antenna.

REFERENCES

[1] A. O. Adeyemi-Ejeye, M. Alreshoodi, L. Al-Jobouri, M. Fleury, and J. Woods, "Packet loss visibility across sd, hd, 3d, and uhd video streams," *Journal of Visual Communication and Image Representation*, vol. 45, pp. 95–106, 2017.

[2] V. Kulshrestha and K. R. Jagdale, "Disruptive technology directions for 6g," in *Towards Wireless Heterogeneity in 6G Networks*, pp. 18–32, CRC Press, 2024.

[3] B. Schultz, "802.11 ad–wlan at 60 ghz–a technology introduction," *Rohde & Schwarz*, 2013.

[4] R. C. Daniels and R. W. Heath, "60 ghz wireless communications: Emerging requirements and design recommendations," *IEEE Vehicular technology magazine*, vol. 2, no. 3, pp. 41–50, 2007.

[5] B. Y. Toh, R. Cahill, and V. F. Fusco, "Understanding and measuring circular polarization," *IEEE Transactions on Education*, vol. 46, no. 3, pp. 313–318, 2003.

[6] S. Kamal, U. Ullah, and S. Koziel, "Excitation of circularly polarized wave via single-feed metasurface-integrated compact antenna for internet of things," *AEU-International Journal of Electronics and Communications*, p. 155196, 2024.

[7] A. O. Martinez, P. Popovski, J. Ø. Nielsen, and E. De Carvalho, "Experimental study of the benefits of a second antenna at the user side in a massive mimo system," *Ieee Access*, vol. 6, pp. 2899–2907, 2017.

[8] S. Kamal, M. F. Ain, U. Ullah, and M. F. M. Omar, "Enabling mimo antenna miniaturization and wide circular polarization coverage by amalgamation of a dielectric strip between meandered traces and slotted ground," *IEEE Antennas and Wireless Propagation Letters*, vol. 21, no. 9, pp. 1901–1905, 2022.

[9] K. Srividhya and P. Jothilakshmi, "Compact coradiator dual polarized mimo antenna for future 5g, emerging 6g and iot applications," *Engineering Science and Technology, an International Journal*, vol. 51, p. 101609, 2024.

[10] S. Kamal and P. Sen, "Microstrip-ministered proximity-coupled stacked dual-port antenna for 6g applications," *IEEE Access*, 2024.

[11] B. Li, Y. Wang, J. Zhao, and J. Shi, "Ultra-wideband antennas for wireless capsule endoscope system: A review," *IEEE Open Journal of Antennas and Propagation*, 2024.

[12] P. Sen, A. Harutyunyan, M. Umar, and S. Kamal, "Joint communication and radar sensing: Rf hardware opportunities and challenges—a circuits and systems perspective," *Sensors*, vol. 23, no. 18, p. 7673, 2023.

[13] K. Thormann and M. Baum, "Single-frame radar odometry incorporating bearing uncertainty," in *2023 IEEE Symposium Sensor Data Fusion and International Conference on Multisensor Fusion and Integration (SDF-MFI)*, pp. 1–7, IEEE, 2023.

[14] Y. Al-Alem and A. A. Kishk, "Low-profile low-cost high gain 60 ghz antenna," *IEEE Access*, vol. 6, pp. 13376–13384, 2018.

[15] S. Kamal, M. F. B. Ain, U. Ullah, A. S. Mohammed, R. Hussin, M. F. B. M. Omar, F. Najmi, Z. A. Ahmad, M. F. Ab Rahman, M. N. Mahmud, *et al.*, "A low-profile quasi-loop magneto-electric dipole antenna featuring a wide bandwidth and circular polarization for 5g mmwave device-to-device communication," *Journal of Electromagnetic Engineering and Science*, vol. 22, no. 4, pp. 459–471, 2022.

[16] Q.-D. Cao, X.-X. Yang, F. Yu, and S. Gao, "High scanning rate millimeter wave circularly polarized cts leaky-wave antenna," *IEEE Transactions on Antennas and Propagation*, 2024.

[17] T. Zhang, L. Li, H. Xia, X. Ma, and T. J. Cui, "A low-cost and high-gain 60-ghz differential phased array antenna in pcb process," *IEEE Transactions on Components, Packaging and Manufacturing Technology*, vol. 8, no. 7, pp. 1281–1291, 2018.

[18] D. G. Kam, D. Liu, A. Natarajan, S. K. Reynolds, and B. A. Floyd, "Organic packages with embedded phased-array antennas for 60-ghz wireless chipsets," *IEEE transactions on components, packaging and manufacturing Technology*, vol. 1, no. 11, pp. 1806–1814, 2011.

[19] Y.-C. Wang and J. A. Okoro, "Impedance calculations for modified coplanar waveguides," *International Journal of Electronics Theoretical and Experimental*, vol. 68, no. 5, pp. 861–875, 1990.

[20] H. Kaupp, "Characteristics of microstrip transmission lines," *IEEE transactions on electronic computers*, no. 2, pp. 185–193, 1967.

[21] Z. J. Silva, C. R. Valenta, and G. D. Durgin, "Design and characterization of meshed microstrip transmission lines," in *2019 IEEE MTT-S International Microwave Symposium (IMS)*, pp. 811–814, IEEE, 2019.

[22] C. A. Balanis, *Advanced engineering electromagnetics*. John Wiley & Sons, 2012.

[23] S. Blanch, J. Romeu, and I. Corbella, "Exact representation of antenna system diversity performance from input parameter description," *Electronics letters*, vol. 39, no. 9, pp. 705–707, 2003.

[24] B. M. Verona, E. Simionato, G. Palomino, I. Aldaya, R. A. Penchel, A. L. Serrano, and G. P. Rehder, "Implementation of a millimeter-wave butler matrix on metallic nanowires-filled membrane platform," *IEEE Access*, 2024.

[25] J. Zhu, S. Liao, S. Li, and Q. Xue, "60 ghz wideband high-gain circularly polarized antenna array with substrate integrated cavity excitation," *IEEE Antennas and Wireless Propagation Letters*, vol. 17, no. 5, pp. 751–755, 2018.

[26] O. Sokunbi and A. Kishk, "Millimeter-wave me-dipole array antenna decoupling using a novel metasurface structure," *IEEE Access*, 2023.

[27] K. Pedram, M. Karamirad, and S. M. H. Ranjbaran, "A novel circular polarization mimo antenna in 60 ghz technology," in *2017 IEEE 4th International Conference on Knowledge-Based Engineering and Innovation (KBEI)*, pp. 0335–0338, IEEE, 2017.